

# Molecular Simulation of the Potential of Methane Reoccupation during the Replacement of Methane Hydrate by CO<sub>2</sub>

Chun-Yu Geng,<sup>†,‡</sup> Hao Wen,<sup>\*,†</sup> and Han Zhou<sup>§</sup>

State Key Laboratory of Multi-Phase Complex Systems, Institute of Process Engineering, Chinese Academy of Sciences, No. 1 2nd North Lane, ZhongGuanCun, Beijing 100190, China, Graduate University of Chinese Academy of Sciences, P.O. Box 4588, Beijing 100049, China, and Research Institute of Petroleum Processing, SINOPEC, No.18 Xueyuan Road, Beijing 100083, China

Received: December 29, 2008; Revised Manuscript Received: March 23, 2009

Molecular dynamics simulations and stabilization energy calculations are performed in this work in order to understand the stability of CH<sub>4</sub> hydrate, CO<sub>2</sub> hydrate, and CH<sub>4</sub>–CO<sub>2</sub> mixed hydrate. The model systems of fully occupied type SI CH<sub>4</sub> hydrate, CO<sub>2</sub> hydrate, and CH<sub>4</sub>–CO<sub>2</sub> mixed hydrate are prepared in a simulation box of 2 × 2 × 2 unit cell with periodic boundary conditions. The MD simulation results reveal that the CH<sub>4</sub>–CO<sub>2</sub> mixed hydrate is the most stable one in above three hydrates. The stabilization energy calculations of small and large cavities occupied by CH<sub>4</sub> and CO<sub>2</sub> show that the CO<sub>2</sub> molecule is less suitable for the small cavity because of its larger size compared with the CH<sub>4</sub> molecule but is more suitable for the large cavity. The results in this work can also explain the possibility of CH<sub>4</sub> molecule in reoccupying the small cavity during the replacement of CH<sub>4</sub> hydrate by CO<sub>2</sub>, from the hydrate stability point of view.

## 1. Introduction

Natural gas hydrate (NGH) is expected to be a future energy resource, since the amount of NGH below the ocean floor is more than all of the current fossil fuel sources combined.<sup>1</sup> Methods based on decomposition of hydrate by external stimulations, such as thermal treatment, depressurizing, and adding inhibitors into the hydrate, have been proposed for producing natural gas from NGH.<sup>2</sup> Some researchers have also suggested that the decomposition of NGH could lead to weakening of the ocean floor.<sup>3</sup>

On the other hand, as the increasing anthropogenic carbon dioxide emission contributes to global warming, CO<sub>2</sub> hydrate is becoming a promising form for CO<sub>2</sub> storage that may help to the climate change mitigation.<sup>4</sup> Interest in CO<sub>2</sub> hydrate has intensified because of discussions on the possible disposal of isolating CO<sub>2</sub> from the atmosphere in deep oceans as a means of greenhouse gas emission reduction.<sup>5–7</sup> Therefore, replacement of natural gas from NGH by CO<sub>2</sub> is also a candidate for producing natural gas from NGH and disposal of CO<sub>2</sub>.<sup>8</sup> This process is a favorable way as a long-term storage of CO<sub>2</sub> and enables the ocean floor to remain stable even after recovering the natural gas, because of the same structure of CH<sub>4</sub> and CO<sub>2</sub> hydrates.<sup>9</sup>

The possibility of replacing natural gas by CO<sub>2</sub> from NGH has been investigated. Measurements of three-phase (vapor–liquid–hydrate) equilibria for CO<sub>2</sub>–CH<sub>4</sub>–H<sub>2</sub>O ternary system show that CO<sub>2</sub> hydrate is thermodynamically more stable than CH<sub>4</sub> hydrate below 283 K, since the equilibrium pressure of CO<sub>2</sub> hydrate is lower than that of CH<sub>4</sub> hydrate.<sup>10–12</sup> Further, the Gibbs free energy of the replacement is found to be a negative value from molecular simulation.<sup>13</sup> This thermodynamic evidence supports the replacement in hydrate at appropriate conditions.

Typically, both CH<sub>4</sub> and CO<sub>2</sub> can form hydrates of type structure I (SI) crystallographic structure,<sup>14,15</sup> in which the small cavity is composed of 12 pentagonal faces (a dodecahedral framework) of 20 H<sub>2</sub>O molecules and forms a dodecahedron framework, and the large one is composed of 12 pentagonal faces and two hexagonal faces of 24 H<sub>2</sub>O molecules and forms a tetrakaidecahedron framework. Though measurements using Raman spectroscopy of SI CO<sub>2</sub> hydrate do not show any splitting in the Raman frequencies, buttressing the notion that CO<sub>2</sub> molecules occupy only large cavities,<sup>16</sup> infrared spectra of the double clathrate, such as carbon dioxide–ethylene oxide, suggest that the CO<sub>2</sub> molecules can occupy both the dodecahedron and the tetrakaidecahedron cavities.<sup>17,18</sup> Crystal structure of type SI CO<sub>2</sub> hydrate has been carried out to confirm that CO<sub>2</sub> molecules can occupy both the small and large cavities.<sup>18</sup> Ota et al.<sup>19</sup> presented an experimental study on the replacement of CH<sub>4</sub> in hydrate with liquid CO<sub>2</sub> and used a view cell for visual observation and Raman spectroscopy for analysis. They found that the CH<sub>4</sub> molecules released from hydrate could reoccupy the small cavities.

In this work, the structures and stability of type SI CH<sub>4</sub> and CO<sub>2</sub> hydrates are studied using molecular dynamics (MD) simulations. Previously, Ding et al.<sup>20</sup> have investigated the partly and fully occupied hydrates and observed a similar dissociation behavior except for the stability for the different occupancy of the hydrates; therefore, the fully occupied hydrates can be used in our simulations to avoid influence of the hydrate occupancy. For understanding the potential of CH<sub>4</sub> molecules in reoccupying the small cavities, the stabilities of CH<sub>4</sub> hydrate and CO<sub>2</sub> hydrate at different temperatures are compared with that of the CH<sub>4</sub>–CO<sub>2</sub> mixed hydrate where CH<sub>4</sub> molecules are engaged in small cavities and CO<sub>2</sub> molecules in large cavities. The tendency of small cavity reoccupation can also be understood by comparison of the stabilization energies of the small and large cavities occupied by CH<sub>4</sub> and CO<sub>2</sub>.

\* To whom correspondence should be addressed. E-mail: hwen@home.ipe.ac.cn.

<sup>†</sup> Institute of Process Engineering.

<sup>‡</sup> Graduate University of Chinese Academy of Sciences.

<sup>§</sup> Research Institute of Petroleum Processing.

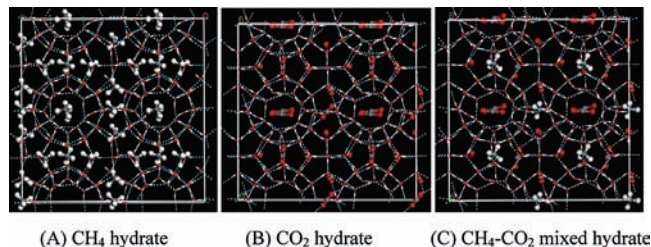


**Figure 1.** Initial configurations of model systems of fully occupied type SI gas hydrates: red for O atoms; light-gray for H atoms; dark-gray for C atoms; light-blue dashed lines for the hydrogen bonding network between H<sub>2</sub>O molecules.

## 2. Simulation Details

**2.1. Simulation Systems and Simulation Methods.** The model systems prepared in this work are fully occupied type SI CH<sub>4</sub> hydrate, CO<sub>2</sub> hydrate, and CH<sub>4</sub>–CO<sub>2</sub> mixed hydrate in a simulation box of  $2 \times 2 \times 2$  unit cell with periodic boundary conditions, as shown in Figure 1. The model system of CH<sub>4</sub> hydrate consists of 64 CH<sub>4</sub> molecules and 368 H<sub>2</sub>O molecules, while CO<sub>2</sub> hydrate consists of 64 CO<sub>2</sub> and 368 H<sub>2</sub>O molecules. The CH<sub>4</sub>–CO<sub>2</sub> mixed hydrate consists of 16 CH<sub>4</sub>, 48 CO<sub>2</sub>, and 368 H<sub>2</sub>O molecules, with CH<sub>4</sub> molecules encaged in small cavities and CO<sub>2</sub> molecules in large cavities. The initial positions of H<sub>2</sub>O molecules in model systems are taken from X-ray diffraction measurements,<sup>21,22</sup> where the gas (CH<sub>4</sub> or CO<sub>2</sub>) molecules are encaged in the center of cavities. Additionally, all atomic positions are allowed to freely translate during the simulation.

The *NPT* ensemble molecular dynamics (MD) simulations are performed with CVFF force field at pressure  $P = 50$  bar and temperatures  $T = 260, 270,$  and  $280$  K, using the Materials Studio software.<sup>23</sup> The temperature and pressure of the model systems are controlled using Andersen<sup>24</sup> and Berendsen<sup>25</sup> methods, respectively. The initial equilibrations of the model systems are optimized by both steepest descent and conjugate gradient. The van der Waals and long-range Coulomb interactions are calculated with the Ewald summation. The Verlet velocity algorithm<sup>26</sup> is used to obtain accurate integrations and statistical ensembles.

Simulation time of 200 ps with an integration time step of 1 fs is typically employed at each temperature, and simulations of the first 50 ps are used for equilibration. The position and orientation of H<sub>2</sub>O molecules are fixed in the first 5 ps simulations during the energy optimization in order to make sufficient movements of the gas molecules. All simulations are performed on the server with Intel Xeon CPU E5335 2.0 GHz and 4G memories.

**2.2. Stabilization Energy of Small and Large Cavities.** Structures of the small and large cavities in type SI hydrate from single crystal X-ray diffraction<sup>21,22</sup> are shown in Figure 2. The small cavity is a dodecahedral framework constructed by 20 H<sub>2</sub>O molecules represented as (5<sup>12</sup>), while the large cavity is a tetrakaidecahedral framework constructed by 24 H<sub>2</sub>O molecules as (5<sup>12</sup>6<sup>2</sup>). The gas molecule occupied cavities are constructed by placing the CH<sub>4</sub> or CO<sub>2</sub> molecule at the center of small and large cavities according to Udachin and IDA et al.'s results,<sup>18,27</sup> represented as CH<sub>4</sub>·(5<sup>12</sup>), CO<sub>2</sub>·(5<sup>12</sup>), CH<sub>4</sub>·(5<sup>12</sup>6<sup>2</sup>), and CO<sub>2</sub>·(5<sup>12</sup>6<sup>2</sup>) in this work for simplification.

The structure optimization of cavities occupied by gas molecules is performed using the hybrid density functional theory in order to compare the stabilization energies of cavities occupied by CH<sub>4</sub> and CO<sub>2</sub>. The hybrid density functional theory

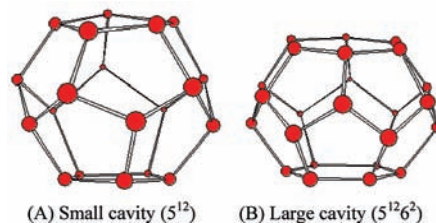


**Figure 2.** Schematic framework of H<sub>2</sub>O molecule cavities in type SI gas hydrates.

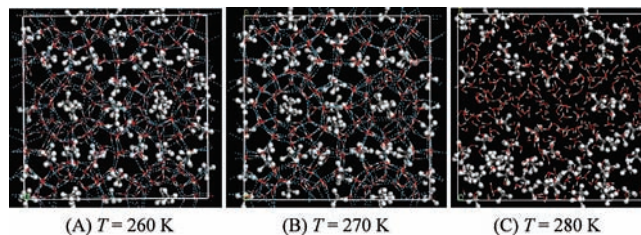


**Figure 3.** Snapshots of the final configurations of CH<sub>4</sub> hydrate at 260, 270, and 280 K.

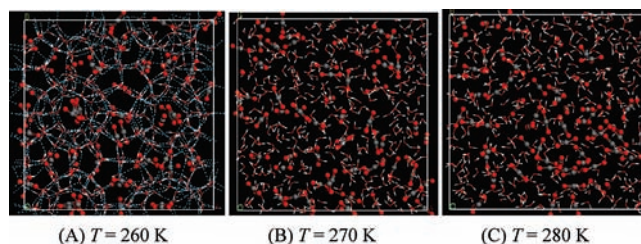


**Figure 4.** Snapshots of the final configurations of CO<sub>2</sub> hydrate at 260, 270, and 280 K.

used in this work is Becke's three-parameter hybrid functional<sup>28</sup> with Lee, Yang, and Parr's correlation functional (B3LYP),<sup>29</sup> using the 6-31g(d,p) basis set. According to ref 30, the stabilization energy of a cavity occupied by a gas molecule is defined as the difference between the total energy of cavities occupied by gas molecules and those of separated H<sub>2</sub>O and gas molecules involved in the cavity occupied by a gas molecule. Thus, in this work, the stabilization energy of cavity occupied by a gas molecule  $\Delta E_{GH}$  can be calculated by

$$\Delta E_{GH} = E_{GH\text{-cavity}} - \sum_i (E_{H_2O})_i - E_{gas} \quad (1)$$

where  $E_{GH\text{-cavity}}$  is the total energy of cavity occupied by gas molecule,  $E_{H_2O}$  and  $E_{gas}$  are the energies of H<sub>2</sub>O and gas molecules involved in the cavity occupied by the gas molecule, respectively.

The aforementioned calculations are performed by using the Gaussian 03 program<sup>31</sup> on the Shenteng 6800 workstation provided by the Computer Network Information Center, Chinese Academy of Sciences.

## 3. Results and Discussion

**3.1. Snapshots of the Final Configurations.** Snapshots of the final configurations of CH<sub>4</sub> hydrate, CO<sub>2</sub> hydrate, and CH<sub>4</sub>–CO<sub>2</sub> mixed hydrate at pressure  $P = 50$  bar and temperatures  $T = 260, 270,$  and  $280$  K are presented in Figures 3–5. Figures 3 and 5 indicate that the crystal structure of CH<sub>4</sub> hydrate and CH<sub>4</sub>–CO<sub>2</sub> mixed hydrate can keep stable at 270 K; even

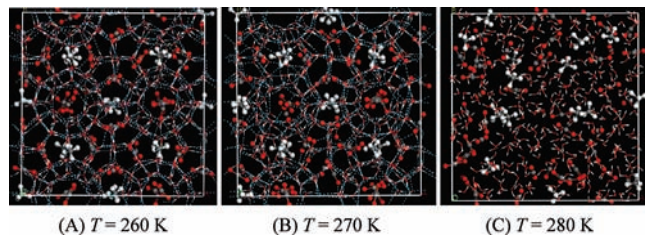


**Figure 5.** Snapshots of the final configurations of CH<sub>4</sub>-CO<sub>2</sub> mixed hydrate at 260, 270, and 280 K.

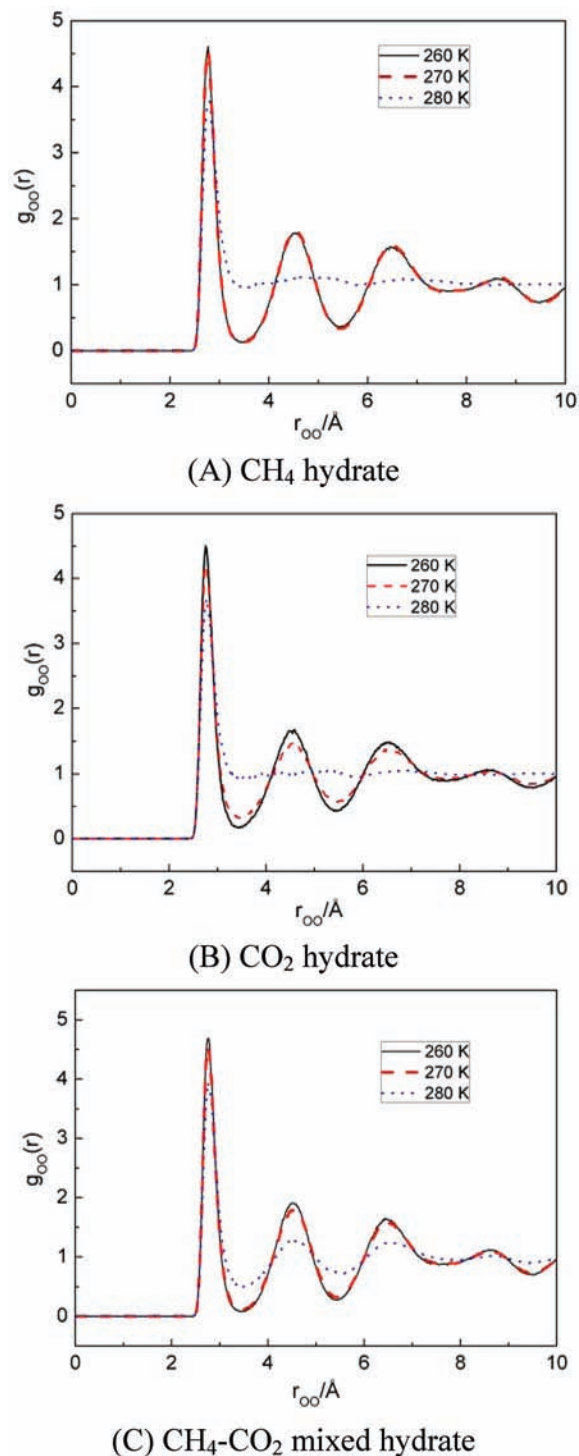
distortions of the hydrogen bonding network between H<sub>2</sub>O molecules appeared. An evident collapse of the hydrogen bonding network in CO<sub>2</sub> hydrate can be observed at 270 K as presented in Figure 4; however, no aggregation of CO<sub>2</sub> molecules observed. When the system temperature grows to 280 K, observable aggregation of CH<sub>4</sub> and CO<sub>2</sub> molecules appears in decomposed CH<sub>4</sub> and CO<sub>2</sub> hydrates. Moreover, the CH<sub>4</sub> molecules exhibit higher aggregation tendency than CO<sub>2</sub> molecules do. While in the CH<sub>4</sub>-CO<sub>2</sub> mixed hydrate, although there are some guest molecules clustering at 280 K, most of the CH<sub>4</sub> and CO<sub>2</sub> molecules are still dispersed in water. Additionally, the average energies of CH<sub>4</sub> hydrate, CO<sub>2</sub> hydrate, and CH<sub>4</sub>-CO<sub>2</sub> mixed hydrate at 280 K are  $-1952.0$ ,  $-2456.5$ , and  $-2549.4$  kcal·mol<sup>-1</sup>, respectively. The result indicates that CH<sub>4</sub>-CO<sub>2</sub> mixed hydrate could be more stable than CH<sub>4</sub> or CO<sub>2</sub> hydrate at the same temperature and pressure.

**3.2. Radial Distribution Function (RDF).** The radial distribution functions (RDFs) of O and C atoms at  $P = 50$  bar and  $T = 260, 270,$  and  $280$  K for CH<sub>4</sub> hydrate, CO<sub>2</sub> hydrate, and CH<sub>4</sub>-CO<sub>2</sub> mixed hydrate are presented in Figures 6 and 7.

In Figure 6, the RDFs of O atom  $g_{OO}(r)$  in H<sub>2</sub>O molecules, for CH<sub>4</sub> hydrate, CO<sub>2</sub> hydrate, and CH<sub>4</sub>-CO<sub>2</sub> mixed hydrate, display a structural consistency with the recent simulations.<sup>32,33</sup> The maximal RDF peaks of the O atom in H<sub>2</sub>O molecules appear at a distance of  $r_{OO} = 2.78$  Å, corresponding to the nearest distance between H<sub>2</sub>O molecules separated from each other at around 2.78 Å. The second maximal peaks appeared at  $r_{OO} = 4.53$  Å and indicate the existence of tetrahedral hydrogen bonding structures of H<sub>2</sub>O molecules in gas hydrates.<sup>20</sup> In Figure 7, the RDF peaks of C atoms in CH<sub>4</sub> and/or CO<sub>2</sub> molecules  $g_{CC}$  appear at  $r_{CC} = 6.7$  Å with excellent agreement with the recent neutron diffraction results and pair correlation functions for gas hydrate.<sup>34</sup> The RDF peaks of C atoms appear at  $r_{CC} = 4.1$  Å and show that the dissociation of hydrates with aggregation of gas molecules occurred when the system temperature rises to 280 K.

It can be seen from Figures 6 and 7 that the gradually lower and broader  $g_{OO}$  peaks at 2.78 and 4.53 Å and  $g_{CC}$  peaks at 6.7 Å with rising temperature indicate the hydrates becoming less stable, while the appearance and growth of  $g_{CC}$  peaks at approximately 4.1 Å imply the aggregation of CH<sub>4</sub> and/or CO<sub>2</sub> molecules. The  $g_{OO}$  and  $g_{CC}$  peaks appearing in CH<sub>4</sub>-CO<sub>2</sub> mixed hydrate are slightly higher than those in CH<sub>4</sub> and CO<sub>2</sub> hydrates at the same temperature and pressure, indicating the higher stability of CH<sub>4</sub>-CO<sub>2</sub> mixed hydrate.

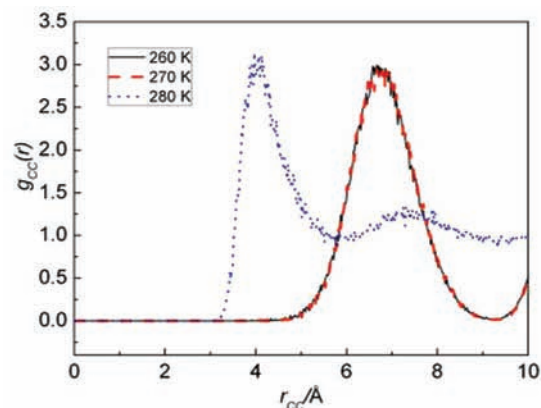
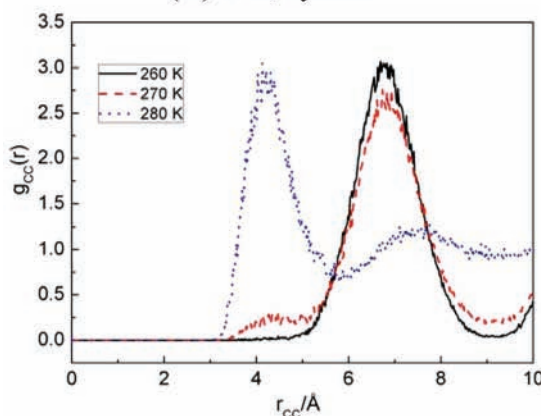
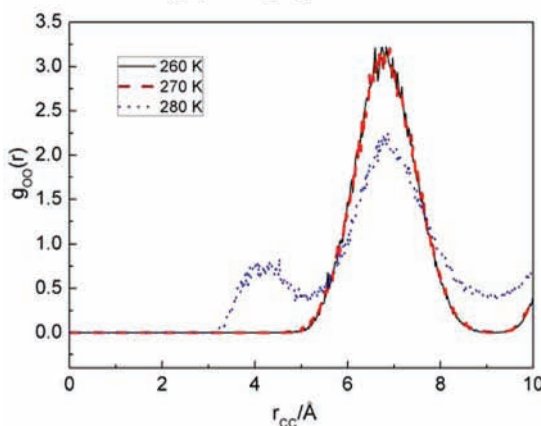
The RDFs of O atom for CH<sub>4</sub> hydrate, CO<sub>2</sub> hydrate, and CH<sub>4</sub>-CO<sub>2</sub> mixed hydrate at  $P = 50$  bar and  $T = 280$  K are presented in Figures 8 and those of the C atom in Figure 9 for further comparison of the stability of different gas hydrates. For RDF peaks of O atoms and those of C atoms at  $r_{CC} = 6.7$  Å, the sharper peak represents the higher hydrate stability while the RDF peaks of C atoms at  $r_{CC} = 4.1$  Å are opposite. The



**Figure 6.** RDFs of O atom in H<sub>2</sub>O molecules at 50 bar and 260, 270, and 280 K for (A) CH<sub>4</sub> hydrate, (B) CO<sub>2</sub> hydrate, and (C) CH<sub>4</sub>-CO<sub>2</sub> mixed hydrate.

CH<sub>4</sub>-CO<sub>2</sub> mixed hydrate exhibits higher stability compared with the CH<sub>4</sub> hydrate and CO<sub>2</sub> hydrate. Although the crystal structure of the CH<sub>4</sub>-CO<sub>2</sub> mixed hydrate decomposes at 280 K, the occurrence of gas-molecule aggregation in the CH<sub>4</sub>-CO<sub>2</sub> mixed hydrate is evidently less than those in CH<sub>4</sub> hydrate and CO<sub>2</sub> hydrate, which can be observed as different by the higher RDF peak of C atoms at 6.7 Å and lower peak at 4.1 Å.

**3.3. Mean Square Displacement (MSD).** The mean square displacement (MSD) is a measure of the average distance a

(A) CH<sub>4</sub> hydrate(B) CO<sub>2</sub> hydrate(C) CH<sub>4</sub>-CO<sub>2</sub> mixed hydrate

**Figure 7.** RDFs of C atom in CH<sub>4</sub> and/or CO<sub>2</sub> molecules at 50 bar and 260, 270, and 280 K for (A) CH<sub>4</sub> hydrate, (B) CO<sub>2</sub> hydrate, and (C) CH<sub>4</sub>-CO<sub>2</sub> mixed hydrate.

molecule travels. For a stable crystal, the constituent molecules vibrate around their lattice sites without diffusing.

Figures 10–12 illustrate the MSD profiles of H<sub>2</sub>O molecules in the CH<sub>4</sub> hydrate, CO<sub>2</sub> hydrate, and CH<sub>4</sub>-CO<sub>2</sub> mixed hydrate at  $P = 50$  bar and  $T = 260, 270,$  and  $280$  K. In Figure 11, it indicates that H<sub>2</sub>O molecules in CO<sub>2</sub> hydrate is slightly diffusing at 270 K, while those in CH<sub>4</sub> hydrate and in CH<sub>4</sub>-CO<sub>2</sub> mixed hydrate still show a typical feature of crystalline solid until the temperature approaches 280 K, as shown in Figures 10 and 12. The collapse of the crystal structure and H<sub>2</sub>O molecule diffusion occurs in the three hydrates when temperature approaches 280 K.

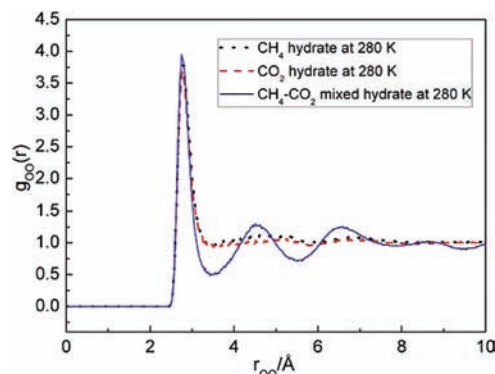


**Figure 8.** RDFs of O atom in H<sub>2</sub>O molecules for CH<sub>4</sub> hydrate, CO<sub>2</sub> hydrate, and CH<sub>4</sub>-CO<sub>2</sub> mixed hydrate at 50 bar and 280 K.

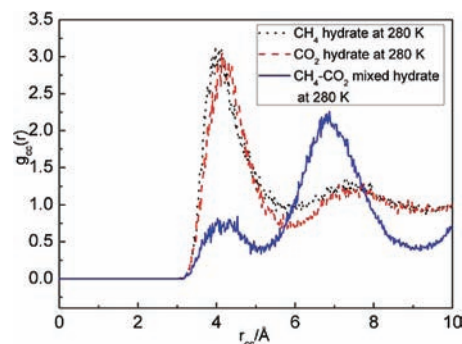


**Figure 9.** RDFs of C atoms in CH<sub>4</sub> and/or CO<sub>2</sub> molecules for CH<sub>4</sub> hydrate, CO<sub>2</sub> hydrate, and CH<sub>4</sub>-CO<sub>2</sub> mixed hydrate at 50 bar and 280 K.

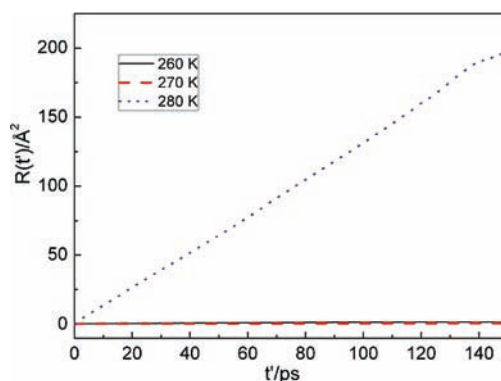


**Figure 10.** MSD of H<sub>2</sub>O molecules in CH<sub>4</sub> hydrate at 50 bar and 260, 270, and 280 K.

A comparison of MSD of H<sub>2</sub>O molecules in the CH<sub>4</sub> hydrate, CO<sub>2</sub> hydrate, and CH<sub>4</sub>-CO<sub>2</sub> mixed hydrate at 270 and 280 K is shown in Figure 13. H<sub>2</sub>O molecules show an obviously larger MSD value in the CO<sub>2</sub> hydrate than those in CH<sub>4</sub> hydrate and in CH<sub>4</sub>-CO<sub>2</sub> mixed hydrate at 270 K. This predicted larger MSD is indicative of partial decomposition of CO<sub>2</sub> hydrate at 270 K. In addition, H<sub>2</sub>O molecules in CH<sub>4</sub> hydrate show larger MSD values than those in CH<sub>4</sub>-CO<sub>2</sub> mixed hydrate do at 280 K, implying that the diffusion of CH<sub>4</sub> hydrate is obviously stronger than the CH<sub>4</sub>-CO<sub>2</sub> mixed hydrate. Accordingly, the decomposition of CH<sub>4</sub> hydrate is much more pronounced than the CH<sub>4</sub>-CO<sub>2</sub> mixed hydrate at 280 K.

Figure 14 presents the predicted diffusion coefficients of CH<sub>4</sub> in the CH<sub>4</sub> hydrate and the CH<sub>4</sub>-CO<sub>2</sub> mixed hydrate and those of CO<sub>2</sub> in CO<sub>2</sub> hydrate and CH<sub>4</sub>-CO<sub>2</sub> mixed hydrate at 260, 270, and 280 K. A comparison of the predicted diffusion coefficients of CH<sub>4</sub> and CO<sub>2</sub> in different hydrates indicates that a significant diffusive motion of the CO<sub>2</sub> hydrate can be

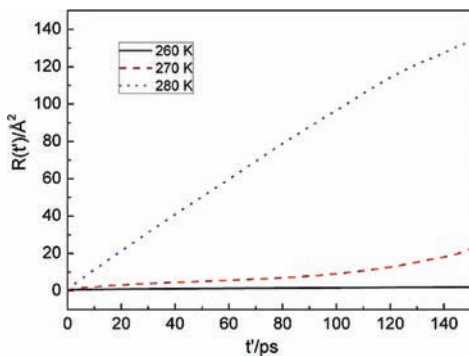


**Figure 11.** MSD of H<sub>2</sub>O molecules in CO<sub>2</sub> hydrate at 50 bar and 260, 270, and 280 K.

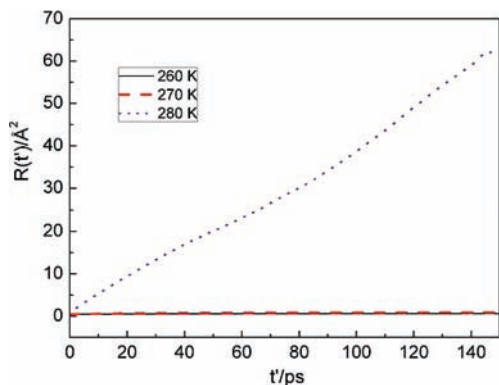


**Figure 12.** MSD of H<sub>2</sub>O molecules in CH<sub>4</sub>-CO<sub>2</sub> mixed hydrate at 50 bar and 260, 270, and 280 K.

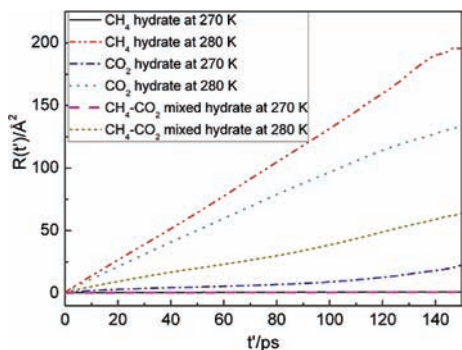


**Figure 13.** MSD of H<sub>2</sub>O molecules in CH<sub>4</sub> hydrate, CO<sub>2</sub> hydrate, and CH<sub>4</sub>-CO<sub>2</sub> mixed hydrate at 270 and 280 K.

observed at 270 K. However, the calculations predict that CH<sub>4</sub> molecules evidently become more diffusive in the CH<sub>4</sub> hydrate at 280 K. Furthermore, at the same temperature, the diffusion is less efficient in the CH<sub>4</sub>-CO<sub>2</sub> hydrate than in the other hydrates. Additionally, the diffusion coefficient of CO<sub>2</sub> hydrate at 273 K in Demurov's result<sup>35</sup> in which 70% of the small cavities are occupied by CO<sub>2</sub> molecules is much lower than that of our fully occupied CO<sub>2</sub> hydrate at 270 K, and it is obviously higher than that of the CH<sub>4</sub>-CO<sub>2</sub> mixed hydrate. The prediction of less efficient diffusion in the mixed hydrate implies that the decomposition of this phase is weaker than either of the others. The result obtained agrees with RDF, which also indicates that the CH<sub>4</sub>-CO<sub>2</sub> mixed hydrate is the most stable hydrate of the three.

**3.4. Stabilization Energies.** Calculations and comparisons on the stabilization energies of CH<sub>4</sub> and CO<sub>2</sub> occupying small and large cavities are performed in an attempt to comprehend the stability of the CH<sub>4</sub> hydrate, the CO<sub>2</sub> hydrate, and the CH<sub>4</sub>-CO<sub>2</sub> mixed hydrate. The small and large cavities of the

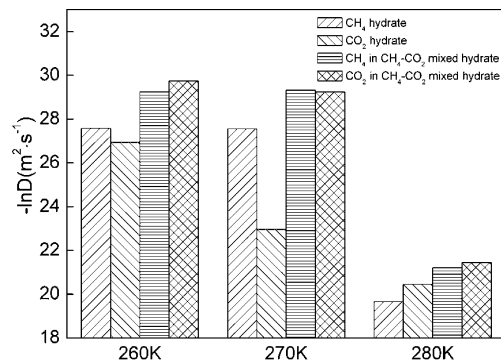


**Figure 14.** Diffusion coefficients of CH<sub>4</sub> and CO<sub>2</sub> molecules in CH<sub>4</sub> hydrate, CO<sub>2</sub> hydrate, and CH<sub>4</sub>-CO<sub>2</sub> mixed hydrate at 260, 270, and 280 K.

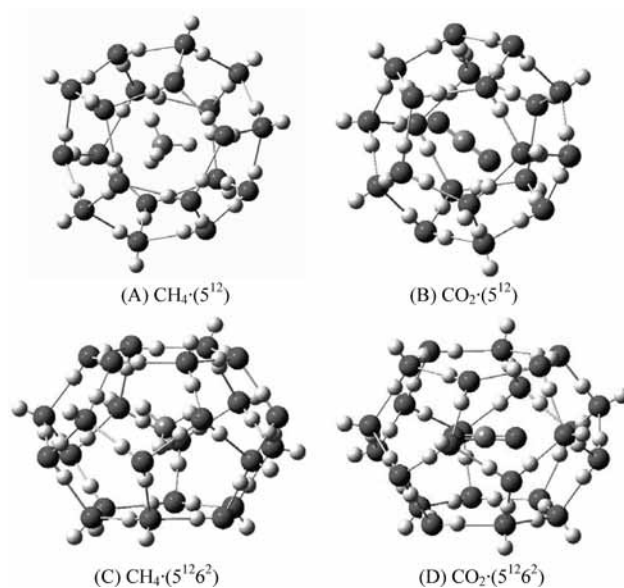


**Figure 15.** Optimized structures of small and large cavities occupied by CH<sub>4</sub> and CO<sub>2</sub>.

hydrate structure from single-crystal X-ray diffraction<sup>21,22</sup> are used as the initial structures for energy optimization. The optimized cavity structures are shown in Figure 15.

For CH<sub>4</sub>·(5<sup>12</sup>) and CO<sub>2</sub>·(5<sup>12</sup>), there are 30 hydrogen-bonding H atoms in each small cavity with average O-H bond length of ~0.99 Å. The average H-O-H bond angle of H<sub>2</sub>O molecule is ~106°. The O-O distance in the dodecahedral structure is 2.73 Å, and the O-O-O angle ~108°. The O-H...O angle is ~176°, and the average bond length of H...O hydrogen bond is 1.75 Å, which represents an effective hydrogen bond. The stabilization energy of CH<sub>4</sub>·(5<sup>12</sup>) is -292.2 kcal·mol<sup>-1</sup>, and that of CO<sub>2</sub>·(5<sup>12</sup>) -285.3 kcal·mol<sup>-1</sup>.

For CH<sub>4</sub>·(5<sup>12</sup>6<sup>2</sup>) and CO<sub>2</sub>·(5<sup>12</sup>6<sup>2</sup>), both of the two cavities have an average O-O distance of ~2.72 Å and O-O-O angle of 110°. There are 36 hydrogen-bonding H atoms in each large cavity. Similarly, the average hydrogen bonding O-H bond length and H-O-H angle of the H<sub>2</sub>O molecule in the large cavity are 0.99 Å and 106°, respectively. The H...O hydrogen bond is ~1.73 Å, and the O-H...O angle 176°. The stabilization energy of CH<sub>4</sub>·(5<sup>12</sup>6<sup>2</sup>) is -357.1 kcal·mol<sup>-1</sup>, and that of CO<sub>2</sub>·(5<sup>12</sup>6<sup>2</sup>) -369.0 kcal·mol<sup>-1</sup>.

The structural parameters of cavities occupied by CH<sub>4</sub> or CO<sub>2</sub> indicate that the gas hydrate cavities do not distort the hydrogen-bonding network, and the size of either small or large cavity is big enough to accommodate a CH<sub>4</sub> or a CO<sub>2</sub> molecule. For

**TABLE 1: Stabilization Energies of Different Clusters<sup>a</sup>**

cluster	$E_{GH-cavity}$ , hartree	$\Delta E_{GH}$ , hartree	$\Delta E_{GH}$ , kcal·mol <sup>-1</sup>
CH <sub>4</sub> ·(5 <sup>12</sup> )	-1569.3537	-0.4657	-292.2
CO <sub>2</sub> ·(5 <sup>12</sup> )	-1717.3996	-0.4546	-285.3
CH <sub>4</sub> ·(5 <sup>12</sup> 6 <sup>2</sup> )	-1875.1299	-0.5691	-357.1
CO <sub>2</sub> ·(5 <sup>12</sup> 6 <sup>2</sup> )	-2023.2058	-0.5880	-369.0

<sup>a</sup> The energies of optimized structures for H<sub>2</sub>O, CH<sub>4</sub>, and CO<sub>2</sub> molecules are -76.4182, -40.5240, and -188.5810 hartree, respectively.

comparison of the stability of cavities occupied by CH<sub>4</sub> and CO<sub>2</sub>, the stabilization energies of CH<sub>4</sub>·(5<sup>12</sup>), CO<sub>2</sub>·(5<sup>12</sup>), CH<sub>4</sub>·(5<sup>12</sup>6<sup>2</sup>), and CO<sub>2</sub>·(5<sup>12</sup>6<sup>2</sup>) are calculated in accordance to eq 1, as presented in Table 1. The calculated stabilization energy of CH<sub>4</sub>·(5<sup>12</sup>) is somewhat larger than Khan's<sup>30</sup> HF and MP2 results, which should be attributed to the different method (B3LYP) used in our calculations. A comparison of the stabilization energy of CH<sub>4</sub>·(5<sup>12</sup>), CO<sub>2</sub>·(5<sup>12</sup>), CH<sub>4</sub>·(5<sup>12</sup>6<sup>2</sup>), and CO<sub>2</sub>·(5<sup>12</sup>6<sup>2</sup>), where the CH<sub>4</sub> and CO<sub>2</sub> molecules are engaged in the small and large cavities, respectively, suggests that CO<sub>2</sub>·(5<sup>12</sup>) is less stable than CH<sub>4</sub>·(5<sup>12</sup>) in the small cavity while CO<sub>2</sub>·(5<sup>12</sup>6<sup>2</sup>) is more stable than CH<sub>4</sub>·(5<sup>12</sup>6<sup>2</sup>) in the large cavity.

Ota et al.<sup>19</sup> reported that during the replacement of CH<sub>4</sub> in the hydrate by use of CO<sub>2</sub>, the decomposition of the large cavity in the CH<sub>4</sub> hydrate proceeded more quickly than that of the small cavity and some portions of the released CH<sub>4</sub> molecules reoccupied the small cavity because the CO<sub>2</sub> molecule is too large to be engaged in the small cavity. Given that CO<sub>2</sub> is somewhat larger than CH<sub>4</sub>, the CO<sub>2</sub>-H<sub>2</sub>O interaction potential in the small cavity should be more repulsive in nature, as seen from the stabilization energies of CH<sub>4</sub>·(5<sup>12</sup>) and CO<sub>2</sub>·(5<sup>12</sup>) that we have calculated. The difference in stabilization energies, as seen from a comparison of the stabilization energies of CH<sub>4</sub>·(5<sup>12</sup>6<sup>2</sup>) and CO<sub>2</sub>·(5<sup>12</sup>6<sup>2</sup>), also suggests that the CO<sub>2</sub> molecule is more suited than the CH<sub>4</sub> molecule to be accommodated in the large cavity. The stabilization energy calculations also support the consideration from MD simulations that the CH<sub>4</sub>-CO<sub>2</sub> mixed hydrate is the most stable of the three hydrates of CH<sub>4</sub>, CO<sub>2</sub>, and CH<sub>4</sub>-CO<sub>2</sub> mixed. Therefore, during the replacement of CH<sub>4</sub> in the hydrate by CO<sub>2</sub>, it is easier to form the CH<sub>4</sub>-CO<sub>2</sub> mixed hydrate because of its stability.

#### 4. Conclusions

The stabilities of the fully occupied type SI CH<sub>4</sub> hydrate, the CO<sub>2</sub> hydrate, and the CH<sub>4</sub>-CO<sub>2</sub> mixed hydrate have been studied by molecular dynamics (MD) simulations at  $P = 50$  bar and  $T = 260, 270,$  and  $280$  K. The final configurations, the radial distribution functions of the O atoms in the H<sub>2</sub>O molecules and the C atoms in CH<sub>4</sub> and CO<sub>2</sub>, the mean square displacements, and the calculated diffusion coefficients of H<sub>2</sub>O, CO<sub>2</sub>, and CH<sub>4</sub> in the various hydrates all indicate that the CH<sub>4</sub>-CO<sub>2</sub> mixed hydrate is the most stable of the three hydrates discussed. The calculation of the structures and the stabilization energies of CH<sub>4</sub> and CO<sub>2</sub> occupying small and large cavities indicate that cavities occupied by CH<sub>4</sub> or CO<sub>2</sub> do not distort the hydrogen-bonding network. A comparison of the stabilization energy indicates that CO<sub>2</sub>·(5<sup>12</sup>) is less stable than CH<sub>4</sub>·(5<sup>12</sup>), whereas CO<sub>2</sub>·(5<sup>12</sup>6<sup>2</sup>) is fairly stable in comparison with CH<sub>4</sub>·(5<sup>12</sup>6<sup>2</sup>).

A comparison of the stabilization energies of the small and large cavities containing CH<sub>4</sub> and CO<sub>2</sub> shows that the CO<sub>2</sub> molecule is less suitable for the small cavity than the CH<sub>4</sub> molecule but is more suitable for the large cavity. Combining

the results from MD simulations with the stabilization energy calculations, one concludes that the CH<sub>4</sub>-CO<sub>2</sub> mixed hydrate exhibits the best stability of the three hydrates considered in this work. In other words, it is possible to form the CH<sub>4</sub>-CO<sub>2</sub> mixed hydrate during the replacement of CH<sub>4</sub> in the hydrate by CO<sub>2</sub>. From the hydrate-stability point of view, the results of this work are consistent with the experimental study by Ota et al.<sup>19</sup> and can also account for the CH<sub>4</sub> reoccupation of the small cavity during the replacement of CH<sub>4</sub> hydrate by CO<sub>2</sub>.

**Acknowledgment.** The authors gratefully appreciate the financial support from the National Natural Science Foundation of China (Grant No. 20821092). The authors also acknowledge generous computational services provided on the Shenteng 6800 workstation referred by the Computer Network Information Center, Chinese Academy of Sciences.

#### References and Notes

- (1) Collett, T. S. *AAPG Bull.* **2002**, *86*, 1971.
- (2) Holder, G. D.; Kamath, V. A.; Godbole, S. P. *Annu. Rev. Energy* **1984**, *9*, 427.
- (3) Gunn, D. A.; Nelder, L. M.; Rochelle, C. A.; Bateman, K.; Jackson, P. D.; Lovell, M. A.; Hobbs, P. R. N.; Long, D.; Rees, J. G.; Schultheiss, P.; Roberts, J.; Francis, T. *Terra Nova* **2002**, *14*, 443.
- (4) Sloan, E. D. *Clathrate Hydrates of Natural Gases*, 2nd ed.; M. Dekker: New York, 1998.
- (5) Herzog, H.; Golomb, D.; Zemba, S. *Environ. Prog.* **1991**, *10*, 64.
- (6) Saji, A.; Yoshida, H.; Sakai, M.; Tani, T.; Kamata, T.; Kitamura, H. *Energy Convers. Manage.* **1992**, *33*, 643.
- (7) Nishikawa, N.; Morishita, M.; Uchiyama, M.; Yamaguchi, F.; Ohtsubo, K.; Kimuro, H.; Hiraoka, R. *Energy Convers. Manage.* **1992**, *33*, 651.
- (8) Ohgaki, K.; Takano, K.; Moritoki, M. *Kagaku Kogaku Ronbunshu* **1994**, *20*, 121.
- (9) Uchida, T.; Ikeda, I. Y.; Takeya, S.; Kamata, Y.; Ohmura, R.; Nagao, J.; Zatssepina, O. Y.; Buffett, B. A. *ChemPhysChem* **2005**, *6*, 646.
- (10) Kang, S. P.; Chun, M. K.; Lee, H. *Fluid Phase Equilib.* **1998**, *147*, 229.
- (11) Anderson, R.; Liamedo, M.; Tohidi, B.; Burgass, W. *J. Phys. Chem. B* **2003**, *107*, 3507.
- (12) Ohgaki, K.; Sangawa, H.; Matsubara, T.; Nakano, S. *J. Chem. Eng. Jpn.* **1996**, *29*, 478.
- (13) Yezdimer, E. M.; Cummings, P. T.; Chialvo, A. A. *J. Phys. Chem. A* **2002**, *106*, 7982.
- (14) Fleyfel, F.; Devlin, J. P. *J. Phys. Chem.* **1988**, *92*, 631.
- (15) Fleyfel, F.; Devlin, J. P. *J. Phys. Chem.* **1991**, *95*, 3811.
- (16) Sum, A. K.; Burruss, R. C.; Sloan, E. D. *J. Phys. Chem. B* **1997**, *101*, 7371.
- (17) Hirai, S.; Okazaki, K.; Kuraoka, S.; Kawamura, K. *Energy Convers. Manage.* **1996**, *37*, 1087.
- (18) Udachin, I. A.; Ratchliffe, C. I.; Ripmeester, J. A. *J. Phys. Chem. B* **2001**, *105*, 4200.
- (19) Ota, M.; Morohashi, K.; Abe, Y.; Watanabe, M.; Smith, R. L., Jr.; Inomata, H. *Energy Convers. Manage.* **2005**, *46*, 1680.
- (20) Ding, L. Y.; Geng, C. Y.; Zhao, Y. H.; Wen, H. *Mol. Simul.* **2007**, *33*, 1005.
- (21) Kirchner, M. T.; Boese, R.; Billups, W. E.; Norman, L. R. *J. Am. Chem. Soc.* **2004**, *126*, 9407.
- (22) Udachin, K. A.; Ratchliffe, C. I.; Ripmeester, J. A. *J. Supramol. Chem.* **2002**, *2*, 405.
- (23) *Materials Studio*, version 4.0; Accelrys Software, Inc.: San Diego, CA, 2006.
- (24) Andersen, H. C. *J. Chem. Phys.* **1980**, *72*, 2384.
- (25) Berendsen, H. J. C.; Postma, J. P. M.; van Gunsteren, W. F.; DiNola, A.; Haak, J. R. *J. Chem. Phys.* **1984**, *81*, 3684.
- (26) Verlet, L. *Phys. Rev.* **1967**, *159*, 98.
- (27) IDA, T.; Mizuno, M.; Endo, K. *J. Comput. Chem.* **2002**, *23*, 1071.
- (28) Becke, A. D. *J. Chem. Phys.* **1992**, *97*, 9173.
- (29) Lee, C.; Yang, W.; Parr, R. G. *Phys. Rev. B* **1988**, *37*, 785.
- (30) Khan, A. *J. Chem. Phys.* **1999**, *110*, 11884.
- (31) Frisch, M. J.; Trucks, G. W.; Schlegel, H. B.; Scuseria, G. E.; Robb, M. A.; Cheeseman, J. R.; Montgomery, J. A., Jr.; Vreven, T.; Kudin, K. N.; Burant, J. C.; Millam, J. M.; Iyengar, S. S.; Tomasi, J.; Barone, V.; Mennucci, B.; Cossi, M.; Scalmani, G.; Rega, N.; Petersson, G. A.; Nakatsuji, H.; Hada, M.; Ehara, M.; Toyota, K.; Fukuda, R.; Hasegawa, J.; Ishida, M.; Nakajima, T.; Honda, Y.; Kitao, O.; Nakai, H.; Klene, M.; Li, X.; Knox, J. E.; Hratchian, H. P.; Cross, J. B.; Bakken, V.; Adamo, C.; Jaramillo, J.; Gomperts, R.; Stratmann, R. E.; Yazyev, O.; Austin, A. J.;

Cammi, R.; Pomelli, C.; Ochterski, J. W.; Ayala, P. Y.; Morokuma, K.; Voth, G. A.; Salvador, P.; Dannenberg, J. J.; Zakrzewski, V. G.; Dapprich, S.; Daniels, A. D.; Strain, M. C.; Farkas, O.; Malick, D. K.; Rabuck, A. D.; Raghavachari, K.; Foresman, J. B.; Ortiz, J. V.; Cui, Q.; Baboul, A. G.; Clifford, S.; Cioslowski, J.; Stefanov, B. B.; Liu, G.; Liashenko, A.; Piskorz, P.; Komaromi, I.; Martin, R. L.; Fox, D. J.; Keith, T.; Al-Laham, M. A.; Peng, C. Y.; Nanayakkara, A.; Challacombe, M.; Gill, P. M. W.; Johnson, B.; Chen, W.; Wong, M. W.; Gonzalez, C.; Pople, J. A. *Gaussian 03*, revision C.02; Gaussian, Inc.: Wallingford, CT, 2004.

(32) Chialvo, A. A.; Housa, M.; Cummings, P. T. *J. Phys. Chem. B* **2002**, *106*, 442.

(33) Hirai, S.; Okazaki, K.; Kuraoka, S.; Kaamura, K. *Energy Convers. Manage.* **1996**, *27*, 1087.

(34) Koh, C. A.; Wisbey, R. P.; Wu, X. P.; Westacott, R. E.; Soper, A. K. *J. Chem. Phys.* **2000**, *113*, 6390.

(35) Demurov, A.; Radhakrishnan, R.; Trout, B. L. *J. Chem. Phys.* **2002**, *116*, 702.

JP811474M